Proceedings of the XI DINAME, 28th February-4th March, 2005-Ouro Preto-MG-Brazil
Edited by D. A. Rade and V. Steffen Jr

Reduction of contact forces in a Rotor-Stator-System in case of rubbing through active auxiliary bearing

Alvaro Chavez
Institute of Applied Mechanics, Technical University of Munich
Boltzmannstr. 15, 85747 Garching, Germany
chavez@amm.mw.tum.de

Heinz Ulbrich
Institute of Applied Mechanics, Technical University of Munich
Boltzmannstr. 15, 85747-Garching, Germany
ulbrich@amm.mw.tum.de

Abstract. *The main emphases of this paper are control concepts, which reduce the contact force in case of rubbing between rotor and stator. This is achieved by designing a controller in such a way that the auxiliary bearing (stator) tracks the given rotor trajectory and by activating the controller before the occurrence of the first contact. Then the control system assures smooth transition to the permanent contact condition (full annular rub), so that multi-contacts are avoided and the complete system will be stable.*

Keywords: *Active auxiliary bearing, Rotor-to-stator rubs, Unilateral contact*

1 Introduction

Because of continuous performance increase of turbo machines it comes to rubbing between components of the rotor and the housing. These unwanted rubbing processes are complicated mechanisms which induce vibrations with the consequence of emerging contact forces, causing not only high impact loads, but also a multitude of vibrations with large amplitudes or even instabilities. This can lead to heavy damage of the machine or to complete destruction. In order to avoid this, a method has been investigated with the help of controlled active bearings to minimize the contact forces. An auxiliary bearing exerts control forces on the rotating system, which is connected to the base through electromagnetic actuators. Because of problem specific control strategies multi impacts during rubbing can be avoided and the amplitude of the single impacts can be drastically reduced, which will be shown by numeric simulations.

The mathematical model characterizes the rotor as an elastic shaft which is pivoted over two passive bearings with linear characteristic curves. The theoretical approach takes into account the degrees of freedom of the bending and of the torsion of the rotor. The used rigid-body contact model, which is described as constraints between contact forces and relative kinematics, allows the calculations of the normal and tangential momentum by means of a time-stepping algorithm. The complete equation of motions are being set up as hybrid multi-body systems (HMBS), whereas coupling between rotor and active auxiliary bearing exists only during the appearance of contact forces. The introduced concepts have been validated with numerical computations and are about to be proven experimentally.

Several authors presented control concepts for minimizing the contact forces in rotor systems. For example, Jiang and Ulbrich (2003) developed optimal control for a Laval rotor. His control design bases on a stability investigation, when the system is in full annular rub. This means that the amplitude and the frequency of the vibrations of the rotor and the auxiliary bearing are both the same and constant. Ulbrich *et. al.* (2004) showed that it is possible to reduce the contact force between the flexible rotor and the auxiliary bearing. The controller has been activated before the first contact occurs. Therefore a smooth transition to full annular rub is ensured. Yigit and Christouforou (2000) used a linearized drill model and a quadratic cost functional to cancel vibration from friction between bore hole and drill.

2 Modelling of the equations of motion

The computer model of the overall system is depicted in Fig. 1. It consists of an elastic rotor, which is held by two isotropic ball bearings, an auxiliary bearing connected to electromagnetic actuators, a magnetic bearing to create realistic excitations to the rotor and an asynchronous motor as controlled driving unit.

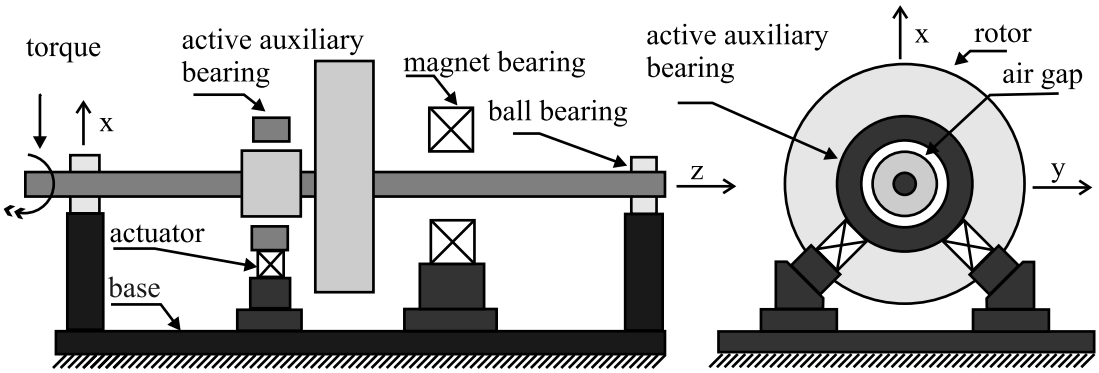

Figure 1: rotor - active auxiliary bearing system

2.1 Rotor

The following assumptions have been made. The rotor has a continuous mass distribution and has been modelled by the Euler-Bernoulli beam theory. The elastic deformation of the beam for bending and torsion are small and of first order. The moment of inertia, inner damping, gyroscopic effects and the rotation symmetry have been accounted for in the mathematical model.

The derivation of the equations of motion of the rotor has been done by the principles of linear and angular momentum. This method grants a modular and physical transparent description also of complex dynamical systems. Description of the rotor system took place in the fixed Cartesian coordinates so that the center line of the shaft lies on the z-axis. To separate the coordinates the Ritz approach has been adopted. The vectors $\mathbf{u}(z)$ and $\boldsymbol{\vartheta}(z)$ are the admissible shape functions with dimensions equal to the numbers of the shape functions. From this follows:

$$\mathbf{M}_r\ddot{\mathbf{q}}_r + (\mathbf{D}_r + \mathbf{G}_r)\dot{\mathbf{q}}_r + (\mathbf{S}_r + \mathbf{N}_r)\mathbf{q}_r = \mathbf{h}_r \tag{1}$$

$\mathbf{M}_r$ consist of mass matrix, $\mathbf{D}_r + \mathbf{G}_r$ is the damping and skew gyroscopic matrix , $\mathbf{S}_r + \mathbf{N}_r$ is the stiffness and the skew circulatory symmetric matrix. The vector $\mathbf{h}_r$ is the generalized outer force. The vector $\mathbf{q}_r(t) = [\mathbf{u}_x^T(t)\ \mathbf{u}_y^T(t)\ \boldsymbol{\vartheta}^T(z)]^T$ is representing the generalized coordinates. The calculation of the matrices is pointed out in detail by Bremer and Pfeiffer (1992), Bremer (1988), Ulbrich (1986) and others.

2.2 Active auxiliary bearing

The schematic of the auxiliary bearing with the actuator is shown in Fig. 1. The active support of the auxiliary bearing is realized by two actuators with a 45^o alignment, whereby the stiffness is rotational symetric. Within these work a electromagnetic actuator is utilized which is completely described in the dissertation of Oberbeck (2002).

The model of this actuator is shown in Fig. 2. The active auxiliary bearing is assumed as a rigid body, which is connected through damper-spring elements at the housing of the actuator to the base, Fig. 1.

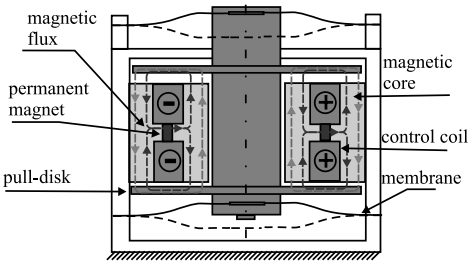

Figure 2: electromagnetic actuator.

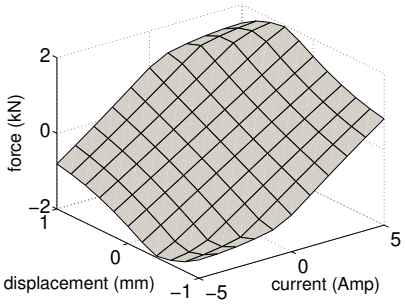

Figure 3: characteristic curve.

The equation of motion of the active auxiliary bearing is

$$\mathbf{M}_f\ddot{\mathbf{q}}_f(t) + \mathbf{D}_f\dot{\mathbf{q}}_f(t) = \mathbf{F}(\mathbf{q}_f, \mathbf{i}) \tag{2}$$

with $\mathbf{q}_f$ as the degree of freedom in x, and y direction. $\mathbf{M}_f$ is the mass matrix of the auxiliary bearing and the actuator. $\mathbf{D}_f$ is the matrix for the outer damping. $\mathbf{F}(\mathbf{q}_f, \mathbf{i})$ is the force vector of the characteristic curve for both actuators.

The characteristic curve of the actuator as it is shown in Fig. 3 depicts the relation between the force, the regulating distance and the coil current. To control these actuators the voltage which is proportional to the coil current is used.

2.3 Contact kinematics

The contact law is being formulated by the non-smooth characteristic curve as described in Pfeiffer and Glocker (1996), Glocker (1995). Following the argumentation of these authors a unilateral contact can be opened or closed during the time dependent process.

When the contact is closed (active contact) a pressure force can be transferred through the contact point. Figure 4 shows a cross section before contact of the auxiliary bearing and the rotor.

In order to analyze the contact kinematics a generalized vector $\mathbf{q}$ with n dimensions is defined. The vectors $\mathbf{q}_r$ and $\mathbf{q}_f$, which are defined by Eq. (1) and (2), respectively have dimensions of $n-2$ and 2.

$$\mathbf{q} = [\mathbf{q}_r^T \ \mathbf{q}_f^T]^T \quad \in \mathbb{R}^n \tag{3}$$

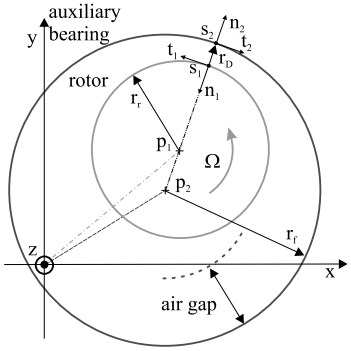

Figure 4: planar contact.

A matrix $\mathbf{J}_{T,f},\ \mathbf{J}_{T,r},\ \mathbf{J}_{R,r}$ is defined as

$$\begin{aligned}
\mathbf{J}_{T,f} &= \begin{bmatrix} \mathbf{0} & \mathbf{0} & \mathbf{0} & 1 & 0 \\ \mathbf{0} & \mathbf{0} & \mathbf{0} & 0 & 1 \\ \mathbf{0} & \mathbf{0} & \mathbf{0} & 0 & 0 \end{bmatrix} && \in \mathbb{R}^{3\times n} \\
\mathbf{J}_{T,r} &= \begin{bmatrix} \mathbf{u}^T(z) & \mathbf{0} & \mathbf{0} & 0 & 0 \\ \mathbf{0} & \mathbf{u}^T(z) & \mathbf{0} & 0 & 0 \\ \mathbf{0} & \mathbf{0} & \mathbf{0} & 0 & 0 \end{bmatrix} && \in \mathbb{R}^{3\times n} \\
\mathbf{J}_{R,r} &= \begin{bmatrix} \mathbf{0} & -\mathbf{u}'^T(z) & \mathbf{0} & 0 & 0 \\ \mathbf{u}'^T(z) & \mathbf{0} & \mathbf{0} & 0 & 0 \\ \mathbf{0} & \mathbf{0} & \boldsymbol{\vartheta}^T(z) & 0 & 0 \end{bmatrix} && \in \mathbb{R}^{3\times n}
\end{aligned} \tag{4}$$

In Equation (4), $\mathbf{J}_{T,r}$ and $\mathbf{J}_{R,r}$ are the translatory and the rotatory Jacobian matrices and $\mathbf{J}_{T,f}$ is the translatory Jacobian matrix of the active auxiliary bearing. $\mathbf{u}(z)$, $\boldsymbol{\vartheta}(z)$ are the vectors of the shape functions of the rotor and $\mathbf{u}'(z)$ the derivation of $\mathbf{u}(z)$.

In Figure 4 is $\delta = |\overrightarrow{P_1P_2}|$ the relative distance, $\mathbf{n}_1$, $\mathbf{t}_1$ normal and tangential vector and $\widetilde{\mathbf{e}_3}$ the basis vector of the z-axis. $\widetilde{\mathbf{a}}\mathbf{b}$ is defined by $\widetilde{\mathbf{a}}\mathbf{b} = \mathbf{a}\times\mathbf{b}$.

$$\begin{aligned}
\delta &= \sqrt{\mathbf{q}^T[\mathbf{J}_{T,r}-\mathbf{J}_{T,f}]^T[\mathbf{J}_{T,r}-\mathbf{J}_{T,f}]\mathbf{q}} \\
\mathbf{n}_1 &= -\delta^{-1}[\mathbf{J}_{T,r}-\mathbf{J}_{T,f}]\mathbf{q} \\
\mathbf{t}_1 &= \widetilde{\mathbf{e}_3}\mathbf{n}_1
\end{aligned} \tag{5}$$

The distance between the contact points (s_1, s_2) in Fig. 4 can be formulated in the following way:

$$\begin{aligned}
g_N &= -\mathbf{r}_D^T\mathbf{n}_1 &&= \delta_0 - \delta \\
\dot{g}_N &= \mathbf{v}_{s1}^T\mathbf{n}_1 + \mathbf{v}_{s2}^T\mathbf{n}_2 &&= -\delta^{-1}\mathbf{q}^T \underbrace{[\mathbf{J}_{T,r}-\mathbf{J}_{T,f}]^T[\mathbf{J}_{T,r}-\mathbf{J}_{T,f}]}_{\mathbf{A}}\dot{\mathbf{q}} \\
\dot{g}_T &= \mathbf{v}_{s1}^T\mathbf{t}_1 + \mathbf{v}_{s2}^T\mathbf{n}_2 &&= \delta^{-1}\mathbf{q}^T \underbrace{[\mathbf{J}_{T,r}-\mathbf{J}_{T,f}]^T\widetilde{\mathbf{e}}_3^T[\mathbf{J}_{T,r}-\mathbf{J}_{T,f}]}_{\mathbf{B}}\dot{\mathbf{q}} + \underbrace{r_r\mathbf{e}_3^T\mathbf{J}_{R,r}}_{\mathbf{c}}\dot{\mathbf{q}}
\end{aligned} \tag{6}$$

g_N is the norm of the distance, $\dot{g}_N$, $\dot{g}_T$ are the norm of the tangential and relative velocity, respectively. After the analysis of the contact kinematics the total differential of Eq. (6) will be discretized (first order Tayler approximation) as already formulated in Stiegelmeyr (2001), Stiegelmeyr and Pfeiffer (1999). The finite difference in the following equation is denoted as Δ.

$$\begin{aligned}
dg_N(\mathbf{q}) &= \underbrace{\frac{\partial g_N}{\partial \mathbf{q}}}_{\mathbf{W}_N^T} d\mathbf{q} && \rightarrow \quad \Delta g_N(\mathbf{q}) &= \mathbf{W}_N^T\Delta\mathbf{q} + O(2) \\
d\dot{g}_N(\dot{\mathbf{q}},\mathbf{q}) &= \underbrace{\frac{\partial \dot{g}_N}{\partial \dot{\mathbf{q}}}}_{\mathbf{W}_N^T} d\dot{\mathbf{q}} + \underbrace{\frac{\partial \dot{g}_N}{\partial \mathbf{q}}}_{\widehat{\mathbf{W}}_N^T} d\mathbf{q} && \rightarrow \quad \Delta\dot{g}_N(\dot{\mathbf{q}},\mathbf{q}) &= \mathbf{W}_N^T\Delta\dot{\mathbf{q}} + \widehat{\mathbf{W}}_N^T\Delta\mathbf{q} + O(2) \\
d\dot{g}_T(\dot{\mathbf{q}},\mathbf{q}) &= \underbrace{\frac{\partial \dot{g}_T}{\partial \dot{\mathbf{q}}}}_{\mathbf{W}_T^T} d\dot{\mathbf{q}} + \underbrace{\frac{\partial \dot{g}_T}{\partial \mathbf{q}}}_{\widehat{\mathbf{W}}_T^T} d\mathbf{q} && \rightarrow \quad \Delta\dot{g}_T(\dot{\mathbf{q}},\mathbf{q}) &= \mathbf{W}_T^T\Delta\dot{\mathbf{q}} + \widehat{\mathbf{W}}_T^T\Delta\mathbf{q} + O(2)
\end{aligned} \tag{7}$$

$$\begin{array}{ll} \mathbf{W}_N = -\delta^{-1}\mathbf{A}\mathbf{q} & \mathbf{W}_T = -\delta^{-1}[\mathbf{B}^T\mathbf{q} + \delta\mathbf{c}^T] \\ \widehat{\mathbf{W}}_N = \ \delta^{-1}[\dot{g}_N\mathbf{W}_N - \mathbf{A}\dot{\mathbf{q}}] & \widehat{\mathbf{W}}_T = \ \delta^{-1}[(\dot{g}_T - \mathbf{c}\dot{\mathbf{q}})\mathbf{W}_N + \mathbf{B}\dot{\mathbf{q}}] \end{array} \tag{8}$$

With the help of: $\Delta\mathbf{q} = \mathbf{q}(t+\Delta t) - \mathbf{q}(t) = \mathbf{q}^{l+1} - \mathbf{q}^l$, $\Delta g_N = g_N(\mathbf{q}+\Delta\mathbf{q}) - g_N(\mathbf{q}) = g_N^{l+1} - g_N^l$, $\Delta\dot{g}_N = g_N(\dot{\mathbf{q}}+\Delta\dot{\mathbf{q}}, \mathbf{q}+\Delta\mathbf{q}) - g_N(\dot{\mathbf{q}}, \mathbf{q}) = \dot{g}_N^{l+1} - \dot{g}_N^l$ und $\Delta\dot{g}_T = g_T(\dot{\mathbf{q}}+\Delta\dot{\mathbf{q}}, \mathbf{q}+\Delta\mathbf{q}) - g_T(\dot{\mathbf{q}}, \mathbf{q}) = \dot{g}_T^{l+1} - \dot{g}_T^l$.

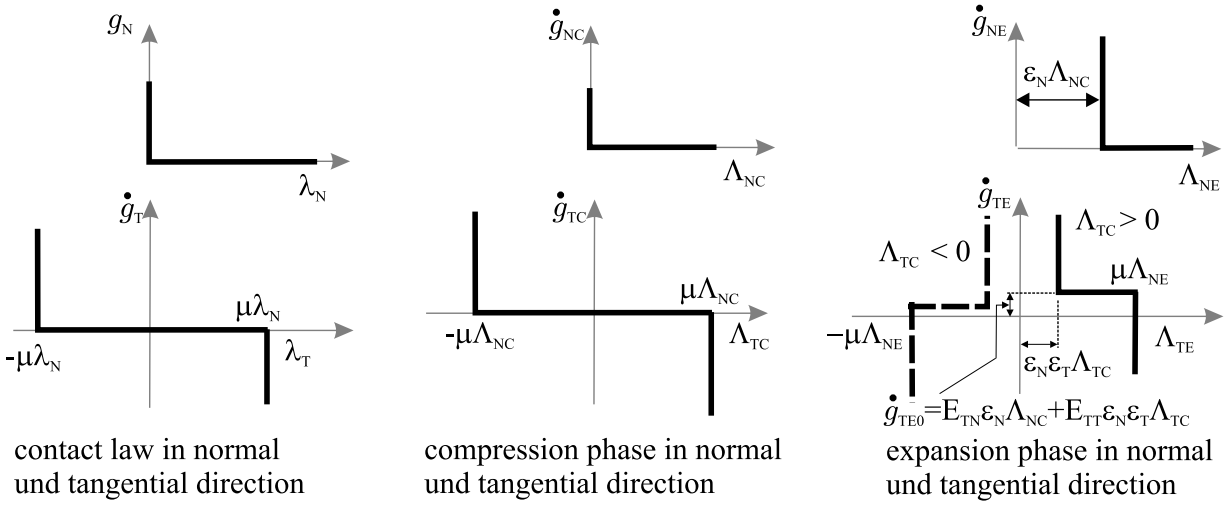

Figure 5: Characteristic line for system with unilateral contact.

2.3.1 Unilateral constrain force

The equation of motion with unilateral contact in a more compact form:

$$\mathbf{M}\ddot{\mathbf{q}} = -\mathbf{h}(\dot{\mathbf{q}}, \mathbf{q}, t) + \mathbf{W}_N\lambda_N + \mathbf{W}_T\lambda_T \tag{9}$$

Here λ_N and λ_T are the normal and tangential force. The vector $\mathbf{W}_N$ and $\mathbf{W}_T$ are the contact vectors from Eq. (8) which projecting the contact forces in the configuration coordinates into the generalized coordinates. The vector $\mathbf{h}$ contains all gyroscopic and active forces as well as all moments and will be defined in the sections below.

The discretization of the acceleration in Eq. (9) is realized through the explicit Euler formula (Eq. 10) and the velocity is discretized by the implicit rule (Eq. 11).

$$\ddot{\mathbf{q}} = \frac{\dot{\mathbf{q}}^{l+1} - \dot{\mathbf{q}}^l}{\Delta t} \tag{10}$$

$$\begin{array}{l} \dot{\mathbf{q}}^{l+1} = \dot{\mathbf{q}}^l + \mathbf{M}^{-1}[\mathbf{h} + \mathbf{W}_N^T\lambda_N + \mathbf{W}_T^T\lambda_T]\Delta t \\ \mathbf{q}^{l+1} = \mathbf{q}^l + \dot{\mathbf{q}}^{l+1}\Delta t \end{array} \tag{11}$$

Equation (9), Eq. (10), Eq. (11) were inserted in Eq. (7) leading to the formula:

$$\begin{bmatrix} g_N \\ \dot{g}_T \end{bmatrix}^{l+1} = \begin{bmatrix} G_{NN}\Delta t & G_{NT}\Delta t \\ G_{TN} & G_{TT} \end{bmatrix} \begin{bmatrix} \Lambda_N \\ \Lambda_T \end{bmatrix} + \begin{bmatrix} \mathbf{G}_N \\ \mathbf{G}_T \end{bmatrix} \mathbf{H}\Delta t + \begin{bmatrix} r_N \\ r_T \end{bmatrix} + \begin{bmatrix} g_N \\ \dot{g}_T \end{bmatrix}^l \tag{12}$$

The forces were multiplied with Δt, $\Lambda_N = \lambda_N\Delta t$, $\Lambda_T = \lambda_T\Delta t$ and $\mathbf{H} = \mathbf{h}\Delta t$. More abbreviations are listed below:

$$\begin{array}{c} \mathbf{G}_N = \mathbf{W}_N^T\mathbf{M}^{-1} \ ; \ \mathbf{G}_T = [\mathbf{W}_T + \widehat{\mathbf{W}}_T\Delta t]^T\mathbf{M}^{-1} \\ G_{NN} = \mathbf{G}_N\mathbf{W}_N \ ; \ G_{NT} = \mathbf{G}_N\mathbf{W}_T \ ; \ G_{TN} = \mathbf{G}_T\mathbf{W}_N \ ; \ G_{TT} = \mathbf{G}_T\mathbf{W}_T \\ r_N = \mathbf{W}_N^T\dot{\mathbf{q}}^l\Delta t \ ; \ r_T = \widehat{\mathbf{W}}_T^T\dot{\mathbf{q}}^l\Delta t \end{array}$$

The calculation of the momentum Λ_N, Λ_T, and accordingly the normal and tangential forces λ_N, λ_T are derived from the left hand side of Fig. 5.

$$\begin{array}{lll} g_N^{l+1} \geq 0 \quad \lambda_N \geq 0 & & g_N^{l+1}\lambda_N = 0 \\ \dot{g}_T^{l+1} = 0 & & \mid \lambda_T \mid -\mu\lambda_N \leq 0 \\ \dot{g}_T^{l+1} \neq 0 & & \lambda_T - sign(\dot{g}_T^{l+1})\ \mu\lambda_N = 0 \end{array} \tag{13}$$

2.3.2 Poisson's impact law

The classical theory of impacts explains them as sudden changes of the motion state of a mass. These impacts are dealt with on the momentum level. Therefore the discretization on the position level is omitted. To do this Eq. (9) is reformulated as an equivalent mass equation.

$$\mathbf{M}d\dot{\mathbf{q}} + d\mathbf{H} - \mathbf{W}_N d\Lambda_N - \mathbf{W}_T d\Lambda_T = \mathbf{0} \tag{14}$$

The discretization of the Eq. (14) has already been done in Stiegelmeyr (2001). The author assumes that the impact time in real systems is finite and therefore the part of the momentum $d\mathbf{H}$ can not be disregarded. Using Poisson's law the impact process will be separated into a compression and an expansion phase. The compression starts at time t_A and ends at t_C. The expansion follows immediately and ends at time t_E. The Equation (14) bases on the discrete compression time $\tau_C = t_C - t_A$, so that $(d \rightarrow \Delta)$.

$$\begin{array}{rcl} \mathbf{M}\underbrace{\Delta\dot{q}}_{\dot{\mathbf{q}}_\mathbf{C}-\dot{\mathbf{q}}_\mathbf{A}} & = & \underbrace{\Delta\mathbf{H}}_{\mathbf{H}_C} + \mathbf{W}_N\underbrace{\Delta\Lambda_N}_{\Lambda_{NC}} + \mathbf{W}_T\underbrace{\Delta\Lambda_T}_{\Lambda_{TC}} \\ \mathbf{q}_C - \mathbf{q}_A & = & \dot{\mathbf{q}}_C\tau_C \end{array} \tag{15}$$

The relative velocity at the end of the compression phase $\dot{\mathbf{g}}_{NC}$, $\dot{\mathbf{g}}_{TC}$, can be calculated analogously to Eq. (12)

$$\begin{bmatrix} \dot{g}_{NC} \\ \dot{g}_{TC} \end{bmatrix} = \begin{bmatrix} C_{NN} & C_{NT} \\ C_{TN} & G_{TT} \end{bmatrix} \begin{bmatrix} \Lambda_{NC} \\ \Lambda_{TC} \end{bmatrix} + \begin{bmatrix} \mathbf{C}_N \\ \mathbf{C}_T \end{bmatrix} \mathbf{H}_C + \begin{bmatrix} r_{NC} \\ r_{TC} \end{bmatrix} + \begin{bmatrix} \dot{g}_A \\ \dot{g}_A \end{bmatrix} \tag{16}$$

With the following shortcuts:

$$\begin{array}{c} \mathbf{C}_N = [\mathbf{W}_N + \widehat{\mathbf{W}_N}\tau_C]^T\mathbf{M}^{-1} \;;\; \mathbf{C}_T = [\mathbf{W}_T + \widehat{\mathbf{W}}_T\tau_C]^T\mathbf{M}^{-1} \\ C_{NN} = \mathbf{C}_N\mathbf{W}_N \;;\; C_{NT} = \mathbf{C}_N\mathbf{W}_T \;;\; C_{TN} = \mathbf{C}_T\mathbf{W}_N \;;\; C_{TT} = \mathbf{G}_T\mathbf{W}_T \\ r_{NC} = \widehat{\mathbf{W}}_N^T\dot{\mathbf{q}}_A\tau_C \;;\; r_{TC} = \widehat{\mathbf{W}}_T^T\dot{\mathbf{q}}_A\tau_C \end{array}$$

The part in the middle of Fig. 5 shows the contact law for the compression phase in normal and tangential contact direction.

$$\begin{array}{lll} \dot{g}_{NC} \geq 0 \quad \Lambda_{NC} \geq 0 & & g_{NC}\Lambda_{NC} = 0 \\ \dot{g}_{TC} = 0 & & \mid \Lambda_{TC} \mid -\mu\Lambda_{NC} \leq 0 \\ \dot{g}_{TC} \neq 0 & & \Lambda_{TC} - sign(\dot{g}_{TC})\ \mu\Lambda_{NC} = 0 \end{array} \tag{17}$$

The relative velocity at the end of the expansion phase $\dot{g}_{NE}$, $\dot{g}_{TE}$ possesses the same structure as in the compression phase in Eq. (16). Swapping of the indices in Eq. (16) $(C \rightarrow E, A \rightarrow C, \tau_C \rightarrow \tau_E)$ with the discrete expansion time $\tau_E = t_E - t_C$, one gets

$$\begin{bmatrix} \dot{g}_{NE} \\ \dot{g}_{TE} \end{bmatrix} = \begin{bmatrix} E_{NN} & E_{NT} \\ E_{TN} & E_{TT} \end{bmatrix} \begin{bmatrix} \Lambda_{NE} \\ \Lambda_{TE} \end{bmatrix} + \begin{bmatrix} \mathbf{E}_N \\ \mathbf{E}_T \end{bmatrix} \mathbf{H}_E + \begin{bmatrix} r_{NE} \\ r_{TE} \end{bmatrix} + \begin{bmatrix} \dot{g}_{NC} \\ \dot{g}_{TC} \end{bmatrix} \tag{18}$$

During the expansion phase Poisson's impact law was used in normal direction with $(\Lambda_{NE} = \varepsilon_N\Lambda_{NC})$. Here ε_N is the dissipation coefficient. The expansion law in tangential direction has been adopted from Beitelschmit (1999). The displacement of the characteristic line on the right side in Fig. 5 of $\varepsilon_N\Lambda_{NC}$ expresses the partly elastic type of the expansion. It is assumed that the contact partners during the expansions can move against each other, without sliding at the contact point. This effect considers the displacement of the left branch of the characteristic line $\varepsilon_N\varepsilon_T\Lambda_{TC}$ with the impact number ε_T $(0 \leq \varepsilon_N \leq 1)$ as the degree of the dissipation of the tangential impact in the expansion phase.

$$\begin{array}{lll} \dot{g}_{NE} \geq 0 & \Lambda_{NE} - \varepsilon_N\Lambda_{NC} \geq 0 & \dot{g}_{NE}(\Lambda_{NE} - \varepsilon_N\Lambda_{NC}) = 0 \\ \dot{g}_{TE} - \dot{g}_{TE0} = 0 & & \varepsilon_N\varepsilon_T \mid \Lambda_{TC} \mid \leq sign(\Lambda_{TC})\ \Lambda_{TE} \leq \mu\Lambda_{NE} \\ \dot{g}_{TE} - \dot{g}_{TE0} > 0 & & \Lambda_{TE} - sign(\Lambda_{TC})\ \varepsilon_N\varepsilon_T \mid \Lambda_{TC} \mid = 0 \\ \dot{g}_{TE} - \dot{g}_{TE0} < 0 & & \Lambda_{TE} - sign(\Lambda_{TC})\ \mu\Lambda_{NE} = 0 \end{array} \tag{19}$$

2.4 Overall system

With the help of

$$\underbrace{\begin{bmatrix} \mathbf{M}_r & \mathbf{0} \\ \mathbf{0} & \mathbf{M}_f \end{bmatrix}}_{\mathbf{M}} \underbrace{\begin{bmatrix} \ddot{\mathbf{q}}_r \\ \ddot{\mathbf{q}}_f \end{bmatrix}}_{\ddot{\mathbf{q}}} + \underbrace{\begin{bmatrix} \mathbf{D}_r + \mathbf{G}_r(\Omega) & \mathbf{0} \\ \mathbf{0} & \mathbf{D}_f \end{bmatrix}}_{\mathbf{D}} \underbrace{\begin{bmatrix} \dot{\mathbf{q}}_r \\ \dot{\mathbf{q}}_f \end{bmatrix}}_{\dot{\mathbf{q}}} + \underbrace{\begin{bmatrix} \mathbf{S}_r + \mathbf{N}_r(\Omega, \dot{\Omega}) & \mathbf{0} \\ \mathbf{0} & \mathbf{0} \end{bmatrix}}_{\mathbf{S}} \underbrace{\begin{bmatrix} \mathbf{q}_r \\ \mathbf{q}_f \end{bmatrix}}_{\mathbf{q}}$$

and

$$\mathbf{h}(\dot{\mathbf{q}}, \mathbf{q}, \mathbf{i}) = \underbrace{-\mathbf{D}\dot{\mathbf{q}} - \mathbf{S}\mathbf{q} + \mathbf{J}_{T,r}^T\, \mathbf{f}_{unw} + \mathbf{J}_{T,r}^T\, \mathbf{f}_{mag}|_{z=z_m} + \mathbf{J}_{R,r}^T\, \mathbf{l}_{dmo}|_{z=z_d}}_{\mathbf{h}_q} + \underbrace{\mathbf{J}_{F,r}^T\, \mathbf{u}_{akt}}_{\mathbf{h}_u}$$

the equation of motion can be described in compact form as

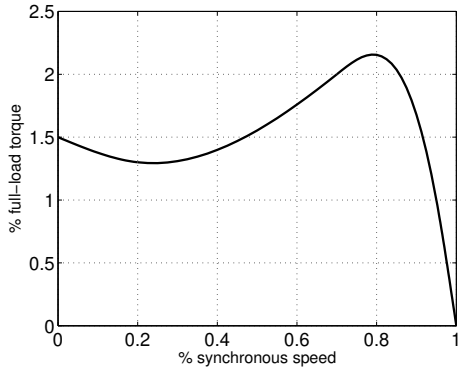

Figure 6: Speed torque curve.

$$\mathbf{M}\ddot{\mathbf{q}} = \underbrace{\mathbf{h}_q + \mathbf{h}_u}_{\mathbf{h}} + \underbrace{\begin{bmatrix} \mathbf{W}_N & \mathbf{W}_T \end{bmatrix}}_{\mathbf{W}} \underbrace{\begin{bmatrix} \lambda_N \\ \lambda_T \end{bmatrix}}_{\boldsymbol{\lambda}} \tag{20}$$

With the mass matrix $\mathbf{M}$, the damping matrix $\mathbf{D}$ and the stiffness matrix $\mathbf{S}$. The vector $\mathbf{h}$, which contains all gyroscopic effects, as well as all active forces and moments, is composed of $\mathbf{h}_q$ and the control force vector $\mathbf{h}_u$. $\mathbf{J}_{T,r}$, $\mathbf{J}_{R,r}$ and $\mathbf{J}_{T,f}$ which have been described in Eq. (4) are the Jacobi matrices at the magnetic bearing ($z = z_m$) and at the torque ($z = z_d$) as can be seen in Fig. 1. The constrain matrix is $\mathbf{W}$ and the vector of the contact force is $\boldsymbol{\lambda}$. The characteristic curve of the torque $\mathbf{l}_{dmo}$ is shown in Fig. 6.

3 Control concept

The control concept should not only minimize the contact force but also account for the nonlinearity of the actuator. The design of the controller should provide smooth contacts to ensure stability while the system is in permanent contact.

$$\mathbf{u}_{akt} = \underset{(\ddot{\mathbf{q}},\dot{\mathbf{q}},\mathbf{q})}{^{arg\ min}} \left\{ \begin{matrix} \mathbf{g}_N \\ \dot{\mathbf{g}}_N \end{matrix} \right. \tag{21}$$

With $arg\ min\ f(x)$ = value of x that minimizes $f(x)$. The $\dot{\mathbf{g}}_T$ will not be take in consideration in Eq. (21) because a non-sliding contact would demand a very high backward whirl compared with the speed of rotation.

3.1 Sliding Control

The main idea of sliding control explained in Khalil (2002), Slotine and Le (1991), Friedland (1996), is the transformation of the problem of tracking error into a problem of stabilizing a time dependent surface, which will be presented in this section.

For designing the controller the mathematical description of the system is taken.

$$\ddot{\mathbf{q}} = \underbrace{\mathbf{M}^{-1}(\mathbf{h}_q + \mathbf{W}\boldsymbol{\lambda})}_{\mathbf{f}} + \underbrace{\mathbf{M}^{-1}\mathbf{J}_{T,f}^T}_{\mathbf{B}}\, \mathbf{u}_{akt} = \mathbf{f}(\dot{\mathbf{q}}, \mathbf{q}, t) + \mathbf{B}\mathbf{u}_{akt} \tag{22}$$

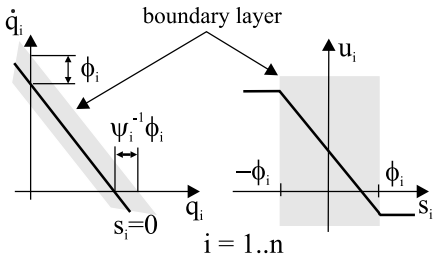

Figure 7: Time variant surface s.

First, introducing the vector $\widetilde{\mathbf{q}} = \mathbf{q} - \mathbf{q}_d$ which defines the error between the generalized coordinates $\mathbf{q}$ and the time variant vector $\mathbf{q}_d$. This leads to

$$\mathbf{Q} = [\ \widetilde{\mathbf{q}}^{\,T}\ \dot{\widetilde{\mathbf{q}}}^{\,T}\ ]^{\,T} \tag{23}$$

Then the time variant surface $\mathbf{s}$ is established. The abbreviation for the diagonal matrix is $diag()$.

$$\mathbf{s}(\mathbf{Q};t) = \dot{\tilde{\mathbf{q}}} + diag(\boldsymbol{\psi})\ \tilde{\mathbf{q}} \tag{24}$$

$diag(\boldsymbol{\psi})$ is a positive-definite matrix. If the conditions $\mathbf{s} \rightarrow \mathbf{0}$ and $\dot{\mathbf{s}} \rightarrow \mathbf{0}$ are met then the stabilization of the surface s can be assured. The calculation of s can be done after the reorganization of Eq. (22) and derivation of Eq. (24). The vector function $\mathbf{f}$ in Eq. (22) is not exactly known because of the parameter λ and is estimated by $\widehat{\mathbf{f}} = \mathbf{M}^{-1}\mathbf{h}_q$. The best approximation to a continuously control law is

$$\widehat{\mathbf{u}}_{akt} = \mathbf{B}^T\mathbf{M}(-\widehat{\mathbf{f}} + \ddot{\mathbf{q}}_d - diag(\boldsymbol{\psi})\ \dot{\tilde{\mathbf{q}}}) \tag{25}$$

In order to remove the discontinuity along $\mathbf{s}$ (chattering effect) caused by the controller, a boundary layer was defined with the positive- definit matrix $diag(\boldsymbol{\psi})$.

$$\mathbf{B}(t) = \{\mathbf{Q}, \mid \mathbf{s}(\mathbf{Q};t) \mid \leq \boldsymbol{\phi}\} \tag{26}$$

The boundary layer will be attractive if the controller fulfills the following criterions:

$$\left.\begin{array}{l} s_i \geq \quad \phi_i \rightarrow \frac{d}{dt}(s_i - \phi_i) \leq -n_i \\ s_i \leq -\phi_i \rightarrow \frac{d}{dt}(s_i - \phi_i) \geq \ n_i \end{array}\right\} \quad \dot{\mathbf{s}} \leq diag(\boldsymbol{\phi} - \mathbf{n})\ sign(\mathbf{s}) \tag{27}$$

With $\mathbf{k} = \mid \mathbf{f}(\mathbf{q}) - \widehat{\mathbf{f}}(q) \mid$ and $\mathbf{k}_d = \mid \mathbf{f}(\mathbf{q}_d) - \widehat{\mathbf{f}}(\mathbf{q}_d) \mid$ the derivation of the boundary layer is defined as

$$diag(\bar{\mathbf{k}}) = diag(\mathbf{k} - \mathbf{k}_d) + diag(\boldsymbol{\psi})diag(\boldsymbol{\phi})\ ;\ diag(\dot{\boldsymbol{\phi}}) + diag(\boldsymbol{\psi})\ diag(\boldsymbol{\phi}) = diag(\mathbf{k}_d)$$

From this follows the control law

$$\mathbf{u}_{akt} = \widehat{\mathbf{u}}_{akt} - diag(\bar{\mathbf{k}})\ sat(diag(\boldsymbol{\Phi})^{-1}\mathbf{s}) \tag{28}$$

The trajectory inside the boundary layer can be expressed directly in terms of the variable $\mathbf{s}$

$$\frac{1}{2}\frac{d}{dt}\mathbf{s}^T\mathbf{s} \leq -\mathbf{s}^T\mathbf{B}\mathbf{B}^T diag(\bar{\mathbf{k}})diag(\boldsymbol{\Phi})^{-1}\mathbf{s} \tag{29}$$

3.2 Feedback linearization und cross coupled feedback

To compensate the nonlinearity of the actuator a feedback-linearization has been applied. The basic principles are stated in Khalil (2002), Slotine and Le (1991). The so linearized actuator is being used for two applications. Firstly, the actuator is used in connection with the auxiliary bearing to stabilize the system when it comes to rubbing and to minimize contact forces as previously explained. Secondly, it is used to simulate the behavior of a passive rotor-auxiliary bearing system.

The cross coupled feedback is activated after the occurrence of the first small impact. The control law is: $-k(\Omega)\widetilde{\mathbf{e}_3}\mathbf{J}_{T,f}\dot{\mathbf{q}}$. With $\widetilde{\mathbf{e}_3}$, $\mathbf{J}_{T,f}$ and $\dot{\mathbf{q}}$ according to the Eq. (5), Eq. (4), Eq. (3), respectively. The factor k is determinated to provide a smooth transition to the steady state condition in order to avoid multi impacts. Others stabilization contact force concepts can be found in Ulbrich (2004), Jiang und Ulbrich (2003).

4 Numerical results

The rotor-active auxiliary bearing used in the following simulation is shown in Fig. 1. First the rotor is on a steady state orbit with a constant rotatory frequency of 50 Hertz. Then after 100 ms the rotor has passed through five cycles, the magnet bearing is activated and produces a rotor amplitude larger than the air gap (0.5 mm). In order to minimize the impulse (Λ) or rather the contact force (λ) the controller is activated 4 ms before the impacts occurs.

The first five plots (Fig. 8) show the performance of the sliding- and cross coupled feedback controller. The first column presents the reduction of the impulse in the normal- und tangential direction and the stabilization of the contact kinematics. The second column shows the stabilization of the $g_N \rightarrow 0$, $\dot{g}_N \rightarrow 0$ (Eq. 21) in order to minimize the contact force. It can be seen in the last picture, that in case of a passive rotor-auxiliary bearing (rotor rubbing without control), the contact force will guide the rotor system to the unstable state with a heavy coupling between transversal- und torsional vibration.

The left picture of the Fig. 9 shows the course of the control force, as previously mentioned. The active auxiliary bearing tracks the rotors trajectory and then stabilizes thes contact forces. The behaviour of the rotor amplitude in x-axis (with-, without control) is showed in central figure. The last picture shows die coil current in the actuators within a distinct time windows from 0.1 to 0.4 second. The actuators are controlled in such a

way that the active auxiliary bearing behaves as if it would be a ring supported by a symmetrical set of linear springs und dampers.

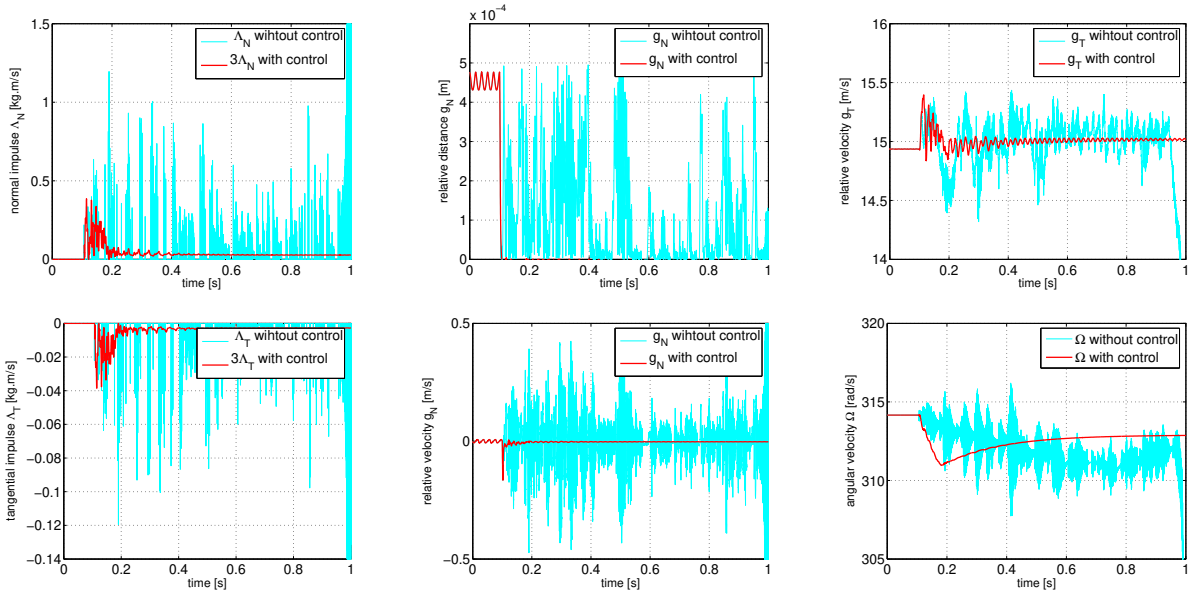

Figure 8: Comparison between the controlled- und uncontrolled system.

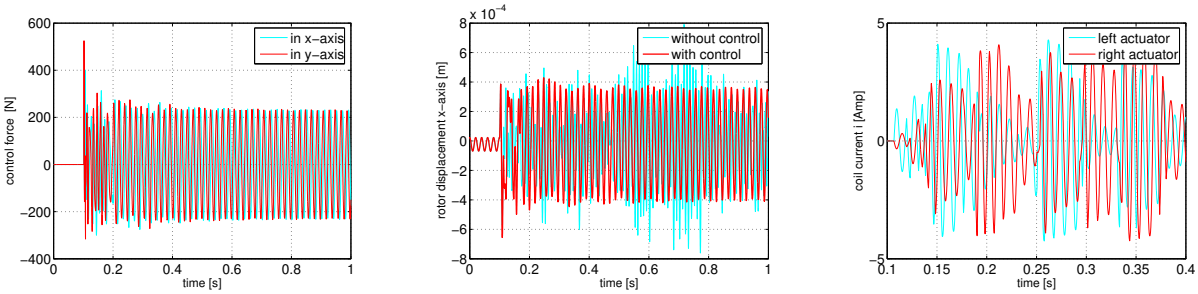

Figure 9: Control force, rotor displacement and current control results.

5 Conclusions and Outlook

This paper dealt with the reduction of contact force in a rotor-stator system. The rotor is modelled as an elastic beam. In addition, an auxiliary bearing, which is connected to electromagnetic actuators has been considered in the model. The torque provided by the drive system follows the speed-torque characteristic of Fig. 6. It accelerates the rotor from zero to full-load speed. The contact process is represented by a rigid body approach with the fundamental property, that for a contact the quantity of the relative kinematics is zero when the corresponding constrain forces is not zero, or vice versa. The integration of the equation of motions is based on a time stepping algorithm.

Numerical results show in case of no constant angular velocity, that the rotor rubbing can result in an unstable state with large relative normal velocity and contact force.

The drive system that ensures a constant angular velocity during the rotor-to-stator rubbing will be take into consideration in the future. Finally, for verification of the theoretical results experiment have to be carried out. These experiments are already in progress. At the TU Munich an experimental set-up has been constructed in order to verify the theorical work and the computer simulation, which have been previously carried out. The designed test rig is showed in Fig. 10.

6 Acknowledgements

The first author is very grateful for the financial support by Deutscher Akademischer Austausch Dienst (DAAD) which makes the research work in this paper possible.

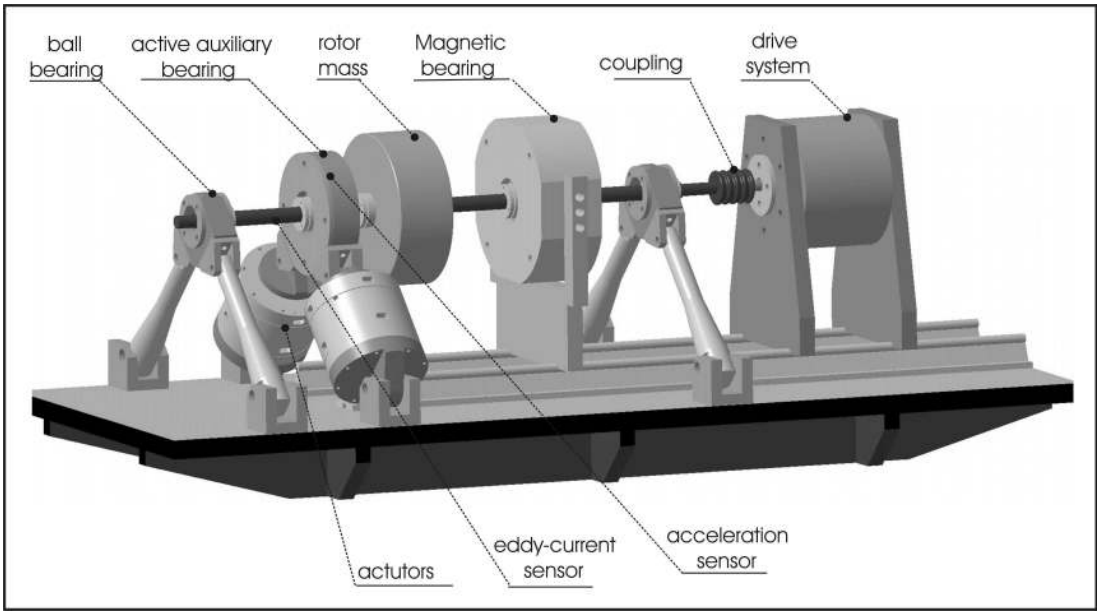

Figure 10: Test rig at TU Munich

References

Beitelschmidt, M., 1999, "Reibstöße in Mehrkörpersystemen", Forstschritt-Berichte VDI, Reihe 11: Schwingungstechnik, No. 275.

Bremer, H., 1988, "Dynamik und Regelung mechanischer Systeme", Teubner Studienbücher, Mechanik 67, ISBN 3-519-02369.

Bremer, H. and **Pfeiffer**, F., 1992, "Elastische Mehrkörpersysteme", Teubner Studienbücher, Mechanik, ISBN 3-519-02374-1.

Friedland, B., 1996, "Advanced Control System Desing", Prentice Hall Publishing, ISBN 0-130-14010-4.

Glocker, C., 1995, "Dynamik von Starrkörpersystemen mit Reibung und Stößen", Forstschritt-Berichte VDI, Reihe 18: Mechanik, Bruchmechanik, No. 82.

Jiang, J.; **Ulbrich**, H., 2003, "Improvement of Rotor Performance under Rubbing Conditions Throught Active Auxiliary Bearing", Proceedings of the 2^{nd} International Symposium on Stability Control of Rotating Machinery, Gdansk, Poland, pp. 160-167.

Khalil, H., 2002, "Nonlinear System", Prentice Hall Publishing, ISBN 0-130-67389-7.

Oberbeck, C., 2003, "Entwicklung und mechatronische Optimierung eines elektromagnestische Aktors", Forstschritt-Berichte VDI, Reihe 8: Meß-, Steuerungs- und Regelungstechnik, No. 984.

Pfeiffer, F. and **Glocker** C., 1996, "Multibody Dynamics With Unilateral Contacts", Jhon Wiley & Sons, Inc., ISBN 0-471-15565-9.

Slotine, J. and **Li** W., 1991, "Applied Nonlinear Control", Prentice Hall Publishing, ISBN 0-130-40890-5.

Stiegelmeyr, A. and **Pfeiffer**, F., 1999, "A Time Stepping Algorithm for Mechanical System With Unilateral Contact", Proceeding of the Desing Engineering Technical Conferences, ASME, VIB-8348, pp. 1-9.

Stiegelmeyr, A., 2001, "Zur numerische Berechnung strukturvarianter Mehrköpersysteme", Forstschritt-Berichte VDI, Reihe 18: Mechanik, Bruchmechanik, No. 271.

Ulbrich, H., 1986, "Dynamik und Rergelung von Rotorsystemen", Forstschritt-Berichte VDI, Reihe 11: Schwingungstechnik, No. 86.

Ulbrich, H. and **Chavez**, A. and **Dhima**, R., 2004, "Minimization of Contact Forces in Case of Rotor Rubbing Using an Actively Controlled Auxiliary Bearing", Proceedings of 10^{th} International Symposium on Transport Phenomena and Dynamics of Rotating Machinery", ID 042, pp. 1-10.

Yigit, A. and **Christorouf**, A., 2000, "Coupled Torsional and Bending Vibration of Actively Controlled Drillstring", Journal of Sound and Vibration, Vol. 234, No. 1, pp. 67-83.